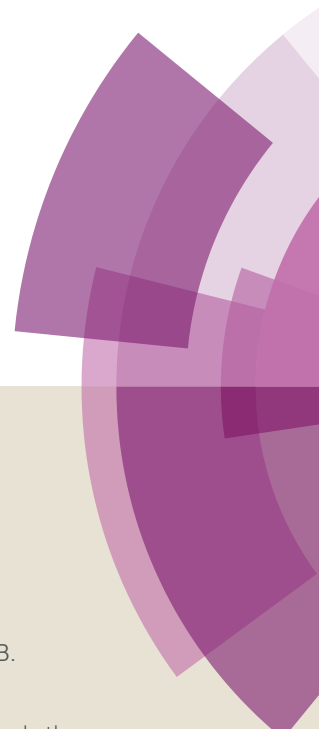


# Dalton Transactions

Accepted Manuscript



This article can be cited before page numbers have been issued, to do this please use: N. Spitsina, M. Blagov, V. Lazarenko, L. Zorina, A. Vasiliev, V. Krapivin, R. Svetogorov, O. Maximova, S. Simonov and E. B. Yagubskii, *Dalton Trans.*, 2019, DOI: 10.1039/C9DT01404G.



This is an Accepted Manuscript, which has been through the Royal Society of Chemistry peer review process and has been accepted for publication.

Accepted Manuscripts are published online shortly after acceptance, before technical editing, formatting and proof reading. Using this free service, authors can make their results available to the community, in citable form, before we publish the edited article. We will replace this Accepted Manuscript with the edited and formatted Advance Article as soon as it is available.

You can find more information about Accepted Manuscripts in the [author guidelines](#).

Please note that technical editing may introduce minor changes to the text and/or graphics, which may alter content. The journal's standard [Terms & Conditions](#) and the ethical guidelines, outlined in our [author and reviewer resource centre](#), still apply. In no event shall the Royal Society of Chemistry be held responsible for any errors or omissions in this Accepted Manuscript or any consequences arising from the use of any information it contains.

## ARTICLE

## Spin-crossover behavior of neutral iron(III) complexes with salicylaldehyde thio-, seleno- and semicarbazone ligands: experiment and theoretical analysis

Received 00th January 20xx,  
Accepted 00th January 20xx

DOI: 10.1039/x0xx00000x

Nataliya G. Spitsyna, <sup>\*a</sup> Maxim A. Blagov, <sup>a,d</sup> Vladimir A. Lazarenko, <sup>b</sup> Leokadiya V. Zorina, <sup>c</sup> Alexander N. Vasiliev, <sup>d,e,f</sup> Vladimir B. Krapivin, <sup>a,b</sup> Roman D. Svetogorov, <sup>b</sup> Olga V. Maximova, <sup>d,e</sup> Sergej V. Simonov, <sup>c</sup> Eduard B. Yagubskii <sup>a</sup>

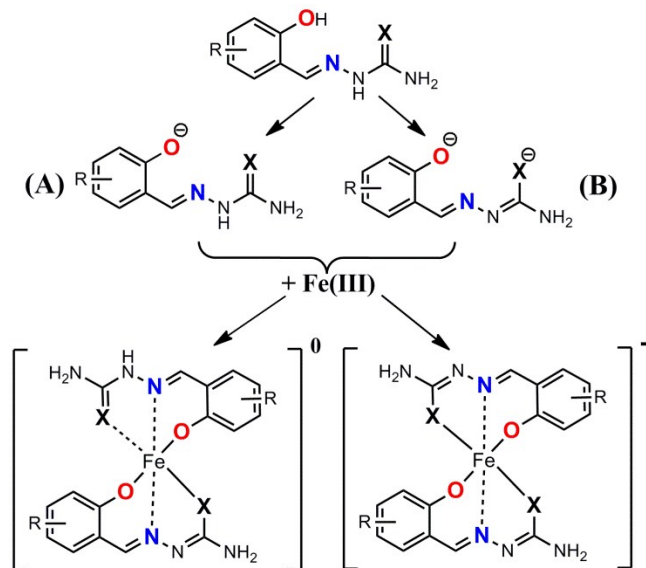
The iron(III) complex [Fe(Hsemsal)(semsal)]·3H<sub>2</sub>O (**1**) (H<sub>2</sub>semsal - salicylaldehyde semicarbazone) has been synthesized and characterized by powder and single crystal X-ray diffraction, and magnetic susceptibility measurements. Crystal structure analysis showed that the complex form neat stacks stabilized by hydrogen-bonding through water molecules and π-π interactions between phenolate rings of ligands. The complex does not exhibit the spin-crossover phenomena and remains in the high-spin state down to 2 K. The DFT calculations were performed for a series of neutral Fe(III) complexes, and the influence of the N<sub>2</sub>S<sub>2</sub>O<sub>2</sub>, N<sub>2</sub>Se<sub>2</sub>O<sub>2</sub> and N<sub>2</sub>O<sub>4</sub> coordination environment on the spin transition in these complexes was traced. The effect of substituents in the benzene ring of salicylaldehyde on stabilization of the HS or LS states in complexes of this type was analyzed.

### Introduction

Compounds exhibiting spin-crossover (SCO) phenomena are routinely observed in *d*<sup>4</sup>–*d*<sup>7</sup> transition metal ions-based compounds, with iron(II/III) complexes being the most common.<sup>1–3</sup> In case of iron(III) (*d*<sup>5</sup>) complexes with specific ligands, thermally induced reversible SCO is associated with the switching between low spin (LS, *S*=1/2) and high spin (HS, *S*=5/2) states of iron(III) ion under temperature change. Noteworthy, the SCO ferric complexes are characterized as more robust with a wide range of choice of ligands. The ability to control the switch between two spin states by external stimuli makes these compounds attractive for applications, e.g. in displays, sensors, molecular switches and information storage devices.<sup>2–8</sup>

Among SCO systems the iron(III) complexes containing two tridentate *O,N,S*-coordinating thiosemicarbazone ligands are

of most interest.<sup>7–11</sup> These ligands are the products of condensation reaction between salicylaldehydes (sal) and thiosemicarbazides (th)/seleno-semicarbazides (se) (for example, H<sub>2</sub>thsal, H<sub>2</sub>sesal, H<sub>2</sub>th5Cl-sal и H<sub>2</sub>th5Br-sal).



**Scheme 1.** Scheme of formation of the neutral and anionic complexes of Fe(III) (X= O, S, Se), where R- is a substitute in the benzene ring of salicylaldehyde. **A** and **B** are mono- and di-anionic forms of ligand, respectively.

Depending on pH of the reaction medium, these ligands can form neutral (**I**) or anionic (**II**) iron(III) coordinated

<sup>a</sup> Institute of Problems of Chemical Physics, RAS, Chernogolovka, MD 142432, Russia.

<sup>b</sup> National Research Center "Kurchatov institute", Moscow 123182, Russia.

<sup>c</sup> Institute of Solid State Physics, RAS, Chernogolovka, MD 142432, Russia.

<sup>d</sup> Lomonosov Moscow State University, Moscow 119991, Russia.

<sup>e</sup> National University of Science and Technology "MISIS", Moscow 119991, Russia.

<sup>f</sup> National Research South Ural State University, Chelyabinsk 454080, Russia.

Electronic Supplementary Information (ESI) available: Photo of the crystalline sample of **1** (Figure S1); TGA curve (Figure S2); XRPD patterns (Figure S3), observed and simulated for **1**; experimental and calculated FT-IR spectra for the H<sub>2</sub>semsal (Figure S4); selected experimental and calculated IR vibrational modes of H<sub>2</sub>semsal (Figure S5); molecular structures of anionic complexes with N<sub>2</sub>O<sub>4</sub> coordination environment (Figure S6); energy-level diagram of  $\alpha$ -spin MOs for Fe(III) neutral complexes (Figure S7); Tables S1–S5, structural details and comparisons; Tables S6–S35 details of experimental methods, and calculations. See DOI: 10.1039/x0xx00000x

complexes (Scheme 1), which demonstrate unique properties: multistep thermally-induced spin transitions (from 2 to 8 steps), LIESST (light-induced excited-spin-state trapping) effect, anomalous temperature dependence of the real part of the dielectric constant, cooperative SCO behavior and a high  $T_{1/2}$  value up to 260 K.<sup>8,12-23</sup> In addition, thiosemicarbazone and some semicarbazone complexes with transition metal ions demonstrate broad chemotherapeutical and biological activities.<sup>18,19</sup>

In contrast to the Fe(III) complexes with  $H_2thsal$  ( $N_2S_2O_2$ ) ligand family, the structure and magnetic properties of Fe(III) ones with salicylaldehyde semicarbazone ligand ( $H_2semsal$ ,  $N_2O_4$  coordination) have not been substantially studied yet. Several attempts to obtain the single crystals of Fe(III) complexes with  $H_2semsal$  ligand suitable for complete X-ray diffraction analysis appeared to be unsuccessful.<sup>11,19</sup>

Herein we report synthesis and characterization of the iron(III) neutral complex  $[Fe(Hsemsal)(semsal)] \cdot 3H_2O$  (**1**) ( $H_2semsal$  - salicylaldehyde semicarbazone). The DFT calculations were performed and the effects of ligand environment on the spin transition in the iron(III) complexes with  $N_2S_2O_2$ ,  $N_2Se_2O_2$  and  $N_2O_4$  donor sets (Scheme 1) were traced. The influence of substituents in the benzene ring of salicylaldehyde on stabilization of the HS or LS state in these complexes was analyzed.

## Experimental section

### Methods and Materials

Materials were purchased from commercial sources and were used without further purification. For syntheses the Sigma-Aldrich  $Fe(NO_3)_3 \cdot 9H_2O$  reagent grade was used.

The purity of  $H_2semsal$  and complex **1** was verified by determining the carbon, hydrogen, and nitrogen content with a Vario MICRO Cube Elementar GmbH Analysis Service. The samples were prepared in tin boats. All samples were measured at least twice, and the average was used.

### Synthesis

The salicylaldehyde semicarbazone ( $H_2semsal$ ) ligand and  $[Fe(Hsemsal)(semsal)] \cdot 3H_2O$  (**1**) were prepared according to improved procedure described earlier.<sup>11,19,24</sup>

**Synthesis of  $H_2semsal$ .** A mixture of equimolar quantities of salicylaldehyde (16.5 mmol, 2.0 g) with semicarbazide hydrochloride (16.5 mmol, 1.6 g) in methanol (75 ml) was refluxing for 16 hours to give colorless solution and then slowly cooled to room temperature. The  $H_2semsal$  compound as white crystalline precipitate was separated by filtration, washed with methanol and dried *in vacuo* over  $P_2O_5$ . Yield 73 %. Calcd. (found%) for  $H_2semsal$  ( $M_w = 179.18$  g/mol),  $C_8H_9N_3O_2$ : C, 53.63 (54.01); H, 5.03 (5.04); N, 23.46 (23.52) %.

**Synthesis of  $[Fe(Hsemsal)(semsal)] \cdot 3H_2O$  (**1**).** The water (15 ml) solution of  $H_2semsal$  (0.86 mmol, 150 mg) and KOH (1.72 mmol, 97 mg) was stirring at room temperature for 30 min, yielding a yellow solution. Solution of  $Fe(NO_3)_3 \cdot 9H_2O$

(0.43 mmol, 180 mg) in water (5 ml) was added dropwise to the stirred reaction mixture, after then it was stirred at room temperature for 6 hours. The resultant brown precipitate was collected by filtration, washed with water. Recrystallization of the crude solid from acetone afforded black single crystals **1** (see Figure S1), which were collected and dried *in vacuo* over  $P_2O_5$ . Suitable single crystals were chosen for X-ray diffraction. Yield 65 %. Calcd. (found%) for  $[Fe(Hsemsal)(semsal)] \cdot 3H_2O$ , ( $M_w = 465.22$  g/mol)  $C_{16}H_{21}FeN_6O_7$ : C, 41.31 (41.30); H, 4.52 (4.33); N, 18.06 (17.98); Fe, 12.04 (11.66) %. The compound **1** is stable in air, and it was dried *in vacuo* for several hours prior to all characterization. The phase purity of **1** was confirmed by comparison of the simulated and experimental powder diffraction patterns (Figure S3).

### Thermogravimetry and differential scanning calorimetry

The thermal stability of solid sample were investigated by using a NETZSCH (Germany) STA 409 C Luxx thermal analyzer, which allows simultaneous thermogravimetry (TG) and differential scanning calorimetry (DSC) measurements.

### IR spectroscopy

The ATR FT-IR absorption spectra were recorded at a room temperature in the range 4000–400  $cm^{-1}$  (50 scans, resolution 4  $cm^{-1}$ ) using FT-IR Bruker model Vertex 70V spectrometer (Germany). The ATR measurements were performed using Platinum-ATR (Bruker) accessory equipped with a pure diamond crystal. The samples were measured as solids.

### Single-crystal structure determinations

X-ray diffraction data were collected at the X-ray Structural Analysis (XSA) beamline ( $\lambda=0.80246$  Å) of Kurchatov Synchrotron Radiation Source. All data were collected at 100 K and in direct ( $\theta=0^\circ$ ) geometry. In total, ~400 frames were collected with oscillation range of  $1^\circ$  in  $\phi$  scanning mode. Absorption correction was applied by using program Scala.<sup>25</sup>

The data were indexed and integrated by using of iMOSFLM from CCP4 software package.<sup>26</sup> Structure was solved by direct methods (intrinsic phasing) in SHELXT<sup>27</sup> and refined in Olex2 software<sup>28</sup> by a full-matrix least-squares method on  $F^2$  with anisotropic displacement, hydrogens were placed according to geometry and residual electron density peaks.

Crystal data for **1**:  $C_{16}H_{21}FeN_6O_7$ ,  $M_w = 465.24$  g/mol, monoclinic, space group  $P2_1/c$  (no. 14),  $a = 17.587(4)$  Å,  $b = 12.556(3)$  Å,  $c = 9.0534(18)$  Å,  $\beta = 93.77(3)^\circ$ ,  $V = 1994.8(7)$  Å<sup>3</sup>,  $Z = 4$ ,  $T = 100(1)$  K, crystal size  $0.05 \times 0.12 \times 0.12$  mm<sup>3</sup>, synchrotron radiation,  $\lambda = 0.80246$  Å,  $\mu = 1.128$  mm<sup>-1</sup>,  $D_{calc} = 1.549$  g/cm<sup>3</sup>, 21114 reflections measured ( $4.504^\circ \leq 2\theta \leq 61.706^\circ$ ), 4319 unique ( $R_{int} = 0.0668$ ,  $R_{sigma} = 0.0520$ ) which were used in all calculations. The final  $R_1$  was 0.0603 (for 3812 reflections with  $I > 2\sigma(I)$  and 305 parameters refined) and  $wR_2$  was 0.1515 (all data),  $Goof = 1.034$ . Crystallographic data for **1** have been deposited with the Cambridge Crystallographic Data Center, CCDC 1903068. The supplementary crystallographic

data can be obtained free of charge from the Cambridge Crystallographic Data Centre via [http://www.ccdc.cam.ac.uk/data\\_request/cif](http://www.ccdc.cam.ac.uk/data_request/cif).

### X-Ray powder diffraction

X-ray powder diffraction (XRPD) study of the samples was conducted at the XSA beamline of Kurchatov Synchrotron Radiation Source with the use of Belok endstation.<sup>29</sup> The monochromatic synchrotron beam with the wavelength of 0.788 Å (photon energy 15734 eV) was used. Diffraction patterns were collected in a transmission mode with 400 μm beam and the distance between the sample and 2D Rayonix SX165 detector was 120 mm. The sample was placed in a cryoloop of 300 μm in size and rotated around the horizontal axis during the measurement, which made it possible to average the diffraction patterns according to the orientations of the sample. The exposure time was 3-5 minutes. To calibrate the sample-detector distance we need a polycrystalline standard with a known position of the diffraction peaks; in this series of measurements, Na<sub>2</sub>Ca<sub>3</sub>Al<sub>2</sub>F<sub>14</sub> (NAC NIST SRM) powder was used.

The two-dimensional diffraction patterns obtained on the detector were further integrated to the standard form of the dependence of the intensity on the scattering angle  $I(2\theta)$  using the Fit2D program and Dionis software.<sup>30</sup> The adequacy of unit cell and space group was confirmed by the Rietveld method using Jana2006 software.<sup>31</sup>

### Magnetic Measurements

Magnetic properties of [Fe(Hsemsal)(semsal)]·3H<sub>2</sub>O were investigated using the VSM option of "Quantum Design" Physical Properties Measurements System PPMS – 9T on the fine powder sample with mass of about 5 mg placed into the plastic capsule. The temperature dependence of *dc* magnetic susceptibility  $\chi$  of the title compound has been taken at warming in a magnetic field  $B=0.1$  T.

### Computation Details

All calculations were carried out using the Gaussian 09 computational package<sup>32</sup> with B3LYP\*<sup>33</sup> (15% Hartree-Fock exchange) hybrid functional, specially developed by Reiher and co-workers on the base of B3LYP,<sup>34,35</sup> to get more accurate results of the energy splitting between states with different spin multiplicity.<sup>36</sup> Calculations of the iron(III) complexes were performed with an unrestricted wave functions. Molecular geometries and orbitals (MOs), electronic energies ( $E_{el}$ ) and vibrational frequencies were calculated using the 6-311++G(d,p) basis set.<sup>37</sup> Zero point energies ( $E_{ZPV}$ ) for the total energy  $E_0$  ( $E_0 = E_{el} + E_{ZPV}$ ) were obtained by the harmonic oscillator approximation. Natural atomic charges were obtained using the NBO 3.1 module<sup>38</sup> in Gaussian 09. The atomic coordinates for starting geometry of neutral complexes were taken from the single crystal structural data (Scheme 1).<sup>20, this work</sup>

## Results and Discussion

View Article Online  
DOI: 10.1039/C9DT01404G

### Thermal Properties

The thermogravimetric analysis of **1** revealed a mass loss of 9.11% in the temperature range 75–200°C, which corresponds to a loss of ~3 molecules of lattice H<sub>2</sub>O (1·3H<sub>2</sub>O, calcd 9.98%), Figure S2. The next weight-loss step appears at a temperature above 200 °C with an endothermic DSC peak at 280 °C, which corresponds to the decomposition of the complex.

### IR spectra

The comparison IR spectra of the ligand (H<sub>2</sub>semsal) and complex [Fe(Hsemsal)(semsal)]·3H<sub>2</sub>O (Figure 1) indicate that the donor atoms (oxygen from the phenolic hydroxyl and C=O group; nitrogen from azomethine group) are engaged in coordination (Scheme 1). The strong bands at 3465 cm<sup>-1</sup> and 1265 cm<sup>-1</sup> in the IR spectrum of ligand, which are assigned to valence vibrations of the phenolic hydroxyl group (Figures S4 and S5),<sup>39</sup> evolve in the IR spectrum of complex **1** as following: the first one almost disappears and the second shifts toward higher energies 1291 cm<sup>-1</sup>, indicating the involvement of oxygen in the coordination of iron ion. One of the strongest bands of the azomethine group  $\nu(\text{C}=\text{N})$  located at 1586 cm<sup>-1</sup> in the spectrum of ligand shifts about 10 cm<sup>-1</sup> toward higher energies in the case of complex **1**.

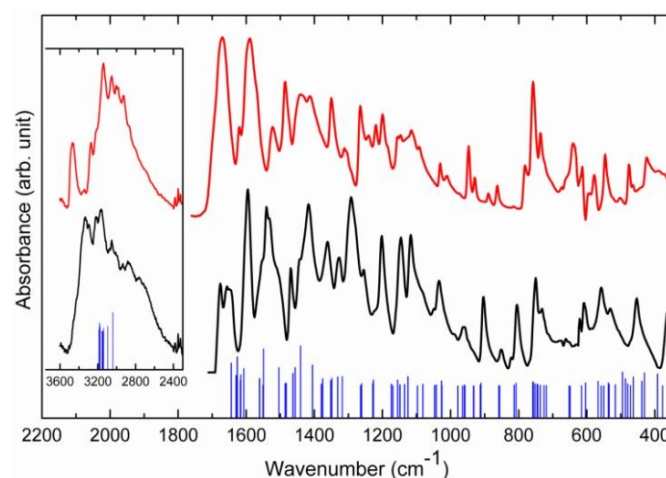


**Figure 1.** Experimental ATR FT-IR absorption spectra for the H<sub>2</sub>semsal (red line) and [Fe(Hsemsal)(semsal)]·3H<sub>2</sub>O (black line),  $T = 293$  K, without preliminary sample preparation. Calculated (B3LYP\*/6-311++G(d,p)) IR vibrational frequencies for the [Fe(Hsemsal)(semsal)] complex in HS state (blue bars).

A very strong band  $\nu(\text{C}=\text{O})$  at 1679 cm<sup>-1</sup> in the ligand spectrum splits into two bands at 1676 cm<sup>-1</sup> (Hsemsal<sup>1</sup>) and 1649 cm<sup>-1</sup> (semsal<sup>2</sup>) in the IR spectrum of **1**. Compared to the spectrum of free ligand, a wide band with a complex structure related to the  $\nu(\text{NH}_2)$  modes is slightly shifted towards higher frequencies in **1** (3400–3000 cm<sup>-1</sup>), Figure 1. Analysis of the IR spectra showed that the ligand chelates the ferric ion in the tridentate manner, as in a number of related anionic

complexes of Fe(III).<sup>20</sup> The complex **1** contains three molecules of crystallization water (see structural description). This correlates with the presence of broad and rather intense absorption bands in the spectral region of 3500–3400 cm<sup>-1</sup> related to the  $\nu(\text{OH})$  modes of water (inset in Figure 1).

### Crystal structure

Complex **1** crystallizes in the monoclinic  $P2_1/c$  space group. The asymmetric unit includes one [Fe<sup>III</sup>(Hsemsal)(semsal)] fragment and three solvent water molecules, all are in general positions.

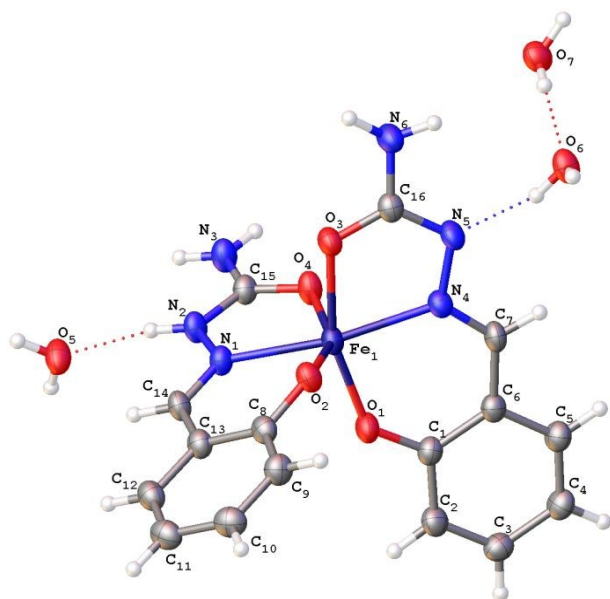


**Figure 2.** Asymmetric unit in **1** with atom numbering scheme (ORTEP drawing with 50% probability ellipsoids).

An ORTEP drawing of **1** is shown in Figure 2, key bond distances and angles are listed in Table 1.

**Table 1.** Selected bond lengths (Å) and angles (°) in [Fe<sup>III</sup>(Hsemsal)(semsal)].

Fe1 O2 1.937(2)	Fe1 O1 1.888(3)
Fe1 O4 2.109(2)	Fe1 O3 2.030(2)
Fe1 N1 2.134(3)	Fe1 N4 2.110(3)
O2 Fe1 O4 154.63(9)	O1 Fe1 O3 161.41(9)
O2 Fe1 N1 84.12(9)	O1 Fe1 N4 86.60(10)
O4 Fe1 N1 73.94(9)	O3 Fe1 N4 75.35(9)
O2 Fe1 N4 111.55(9)	O1 Fe1 N1 96.04(10)
O4 Fe1 N4 89.86(9)	O3 Fe1 N1 102.53(9)
O2 Fe1 O3 86.46(10)	O1 Fe1 O4 98.51(10)
O1 Fe1 O2 96.29(11)	O3 Fe1 O4 86.04(9)
N1 Fe1 N4 163.79(10)	

The Fe(III) ion in the metal complex has a distorted octahedral environment of two nitrogen and four oxygen atoms of two chelating salicylaldehyde semicarbazone ligands. The chelating agents are in two tautomeric forms:

monoanionic keto form with proton at the hydrazinic nitrogen atom N(2) and deprotonated dianionic eno form (Scheme 1). The dianionic ligand forms shorter coordination bonds to the central metal ion in comparison with the monoanionic one (Table 1, maximal difference is 0.07 Å for Fe–O<sub>carbonyl</sub>) whereas all covalent bonds in the semicarbazone moieties are practically identical in both tautomers ( $\pm 0.01$  Å, Table S1). The dianionic semsal ligand is more planar in comparison with monoanionic Hsemsal unit (Figure 3). The dihedral angle between OCN<sub>3</sub> and OC<sub>7</sub> parts of the ligand is 18.02(9)° for Hsemsal and only 2.08(7)° for semsal. The angle between the average Hsemsal and semsal planes in **1** is equal to 84.61(2)°.

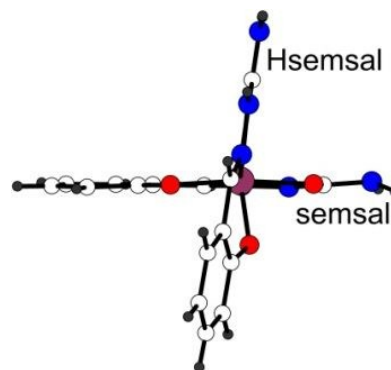


**Figure 3.** Different degree of planarity of Hsemsal and semsal ligands in the complex **1**.

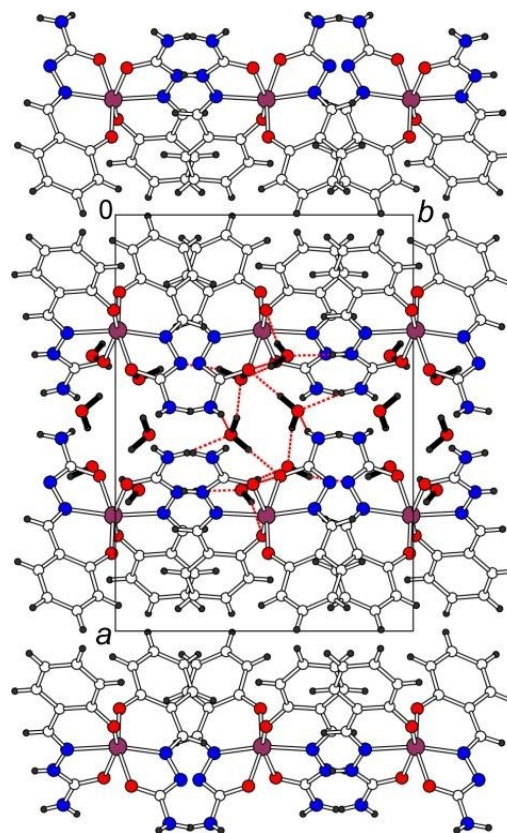


**Figure 4** Projection of the structure **1** along  $c$ . The hydrogen bonding through six H<sub>2</sub>O molecules near (1/2, 1/2, 0) center are shown by red dotted lines.

The bond lengths analysis reveals that the complex **1** is in a high spin state at 100 K. The average bond lengths Fe-N, Fe-O<sub>phenolate</sub> and Fe-O<sub>carbonyl</sub> are 2.123, 1.912 and 2.070 Å, respectively. Previously only one crystallographically characterized phenolic semicarbazone complex of Fe(III) has been published.<sup>18</sup> This ferric adamantyl semicarbazone (asc) complex of the [Fe(asc)<sub>2</sub>]ClO<sub>4</sub>·0.5EtOH composition is in HS state and fully protonated at the hydrazinic nitrogens. The Fe-N (2.109(3) Å) and Fe-O average bond lengths (phenolate 1.902(2) Å and carbonyl 2.090(4) Å) are very similar to the corresponding values in **1**. The HS complexes of Fe(III) are also characterized by noticeable distortion of the coordination octahedron: the O-Fe-O and N-Fe-N angles in **1** differ from 180° (Table 1). In the related low-spin complexes of Fe(III) with hydrazone or thiosemicarbazone ligands the central octahedron has much less distortion and the lengths of Fe-ligand bonds are shorter by 0.1-0.3 Å.<sup>20,21</sup>

stacks: stack 1 is composed of Hsemsal units, stack 2 consists of semsal units (Figure 5). The stacks are slightly different from each other. The interplane angle is 12.22(7)° and 40.02(6)° in the stack 1 (Figure 5b) and 2 (Figure 5c), respectively. The average distances between the planes are 3.04 Å in 1 and 3.51 Å in 2. The stack 1 with less interplane angle has larger amount of shortened C...C contacts than the stack 2 (the contacts < 3.6 Å are shown by dotted lines in Figure 5a).

**Table 2.** Hydrogen bonds geometry in **1**.

D	H	A	d(D-H)/Å	d(H-A)/Å	d(D-A)/Å	D-H-A/°
N2	H2	O5	0.80(4)	1.91(4)	2.708(4)	178(4)
N3	H3B	O7 <sup>1</sup>	0.84(5)	2.05(5)	2.871(4)	168(4)
N6	H6B	O7 <sup>2</sup>	0.90(3)	2.09(3)	2.958(4)	162(4)
O5	H5A	O6 <sup>3</sup>	1.03(5)	1.73(5)	2.748(3)	172(4)
O5	H5B	O2 <sup>4</sup>	0.93(5)	1.92(5)	2.823(4)	163(4)
O6	H6C	N5	1.01(5)	1.74(5)	2.725(3)	164(4)
O6	H6D	O4 <sup>2</sup>	0.90(5)	1.94(5)	2.790(3)	158(4)
O7	H7A	O6	0.95(5)	1.83(5)	2.749(4)	162(4)
O7	H7B	O3 <sup>5</sup>	0.97(5)	1.80(5)	2.768(3)	174(4)

<sup>1</sup>1-x, 1-y, 1-z; <sup>2</sup>x, 0.5-y, 0.5+z; <sup>3</sup>x, 1+y, +z; <sup>4</sup>x, 1.5-y, z-0.5; <sup>5</sup>1-x, y-0.5, 1.5-z

Water molecules (they are marked by thick black bonds in Figure 4) are located in the cavities around (1/2, 1/2, 0) and (1/2, 0, 1/2) centers. They are involved in strong hydrogen bonding both with each other and with surrounding Fe complexes which locks the layers in pairs. In these interactions each of three independent water molecules plays mixed donor-acceptor role in the O-H...O, O-H...N and N-H...O contacts. The hydrogen bonds geometry is described in Table 2. Note that the direct hydrogen bonding between the Fe complexes without water mediation is not observed.

### Magnetic Properties

The temperature dependence of *dc* magnetic susceptibility  $\chi$  of the title compound **1** taken at warming in a magnetic field  $B = 0.1$  T is shown in Figure 6. In the wide temperature range, the  $\chi(T)$  curve follows the Curie-Weiss law with inclusion of the temperature independent term  $\chi = \chi_0 + C/(T - \theta)$ . The fitting of experimental data in the range  $T = 200 - 300$  K results in  $\chi_0 = -1.1 \times 10^{-3}$  emu/mol. This term arises from the combination of diamagnetic Pascal constants of individual atoms in the title compound<sup>40</sup> and weak diamagnetic signal of the sample holder. The Curie constant  $C = 4.57$  emuK/mol corresponds to the expected value for the Fe(III) ions in the high spin state  $S = 5/2$ . Negative value of the Weiss temperature  $\theta = -2.6$  K evidences weak antiferromagnetic interaction between magnetic centers in **1**. The presence of antiferromagnetic interaction between magnetic centers in **1** could occur due to the presence of  $\pi$ -stacking interactions of the ligands of adjacent molecules in the layer (Figures 4 and 5). The

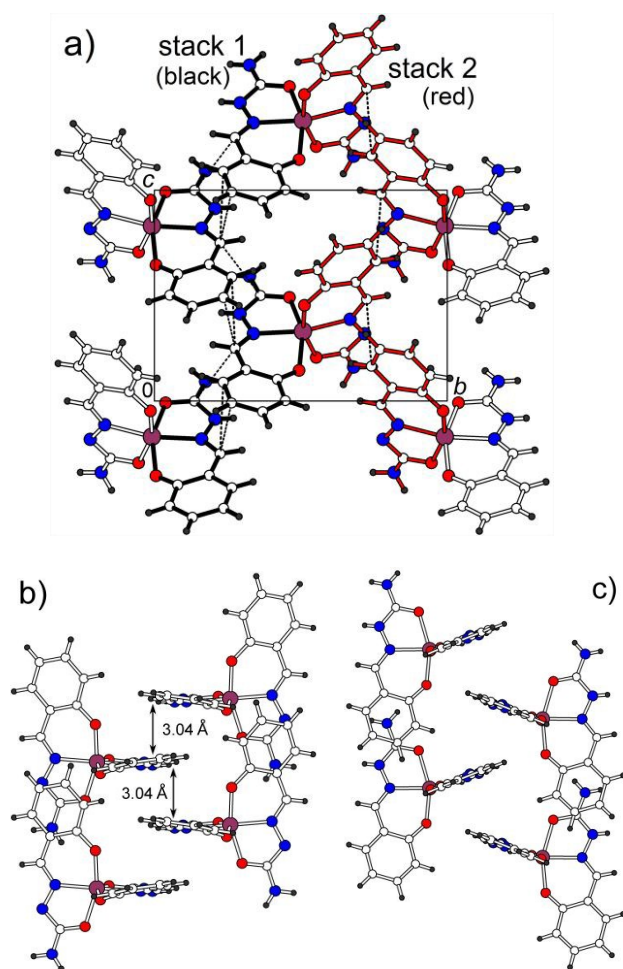


**Figure 5** The *bc* layer (a), stack 1 (b) and stack 2 (c). Intrastack C...C contacts < 3.6 Å are shown by dotted lines.

The [Fe(Hsemsal)(semsal)] units are packed into 2D-layers parallel to the *bc* plane in such a way that in between of two adjacent layers either -NH<sub>2</sub> or phenyl ends of chelating agents are located (Figure 4). Adjacent molecules in the layer interact by  $\pi$ -stacking of the ligands. There are two independent  $\pi$ -

extrapolation of the fitting curve to low temperatures is shown by dashed line in the main panel of Figure 6.

The inset to Figure 6 represents the temperature dependence of  $\chi^*T$  product where  $\chi^* = \chi - \chi_0$  is the magnetic susceptibility corrected for temperature independent diamagnetic contribution. Down to  $\sim 50$  K, the value of this product is almost temperature independent reflecting the constant value of effective magnetic moment  $\mu_{\text{eff}} = (8C)^{1/2}\mu_B$ . Below this temperature, the  $\chi^*T$  product diminishes reflecting presence of weak antiferromagnetic interaction between magnetically active centers. This trend can be reproduced without considering a zero-field splitting of the iron ions.<sup>41</sup>

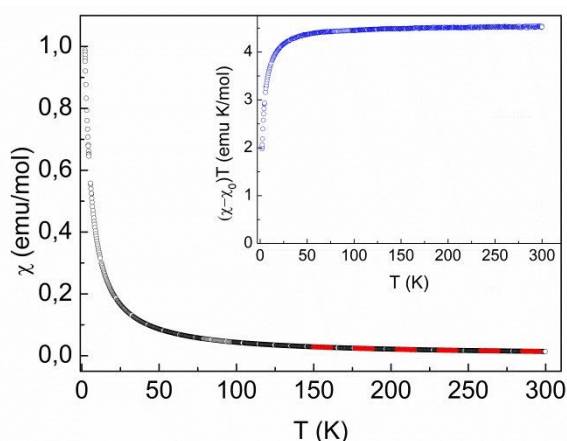


**Figure 6.** The temperature dependence of *dc* magnetic susceptibility  $\chi$  in **1** taken at  $B = 0.1$  T. The dashed line is the fitting by the Curie-Weiss law. The inset represents the temperature dependence of the product  $\chi^*T$ , where  $\chi^* = \chi - \chi_0$ .

Nevertheless, there are some works that reported spin transition in the ferric complexes with  $N_2O_4$  coordinated environment ( $[Fe(\text{azp})_2]$ ,  $H_2\text{azp} = 2,2'$ -azodiphenol;  $[Fe(\text{aznp})_2]$ ,  $H_2\text{aznp} = (2'$ -hydroxyphenylazo)-2-hydroxynaphthalene) (Figure S6).<sup>17</sup> That is unusual, because an oxygen atom belongs to weak field ligands. Spin transition in these complexes is achieved by  $\sigma$ -bonding of nitrogen atom of azo groups ( $-N=N-$ ) to iron *d*-orbitals, that increases a ligand-field splitting energy.<sup>16,17</sup>

### DFT calculations

To determine the influence of coordination  $X_2N_2O_2$  ( $X=O$ ; S; Se (A and B, Scheme 1) environment of Fe(III) neutral complexes on the spin-crossover the DFT calculations were performed. The optimized coordination structures for neutral complexes agree quite well with the corresponding crystal structures. However, experimental bond lengths of Fe-N(A) and Fe-X(A) for neutral complexes ( $R=H$ ) are somewhat different from calculated values. These bond distances might be considerably influenced by the crystal packing.<sup>42</sup> The calculated elongation of the bond lengths in the neutral complexes upon the LS $\rightarrow$ HS transition are following: Fe-N(A) (14.63-13.89 %), Fe-X(A) (10.70-8.08 %), Fe-N(B) (11.13-10.85 %) and Fe-X(B) (6.16-4.94

%), while the increase of Fe-O(A, B) bond length is less pronounced (1.30-4.17 %) (Table S2). This tendency is conformed experimentally for neutral complex  $[Fe(\text{Hth5Br-sal})(\text{th5Br-sal})] \cdot H_2O$  (Table S3).<sup>21</sup>

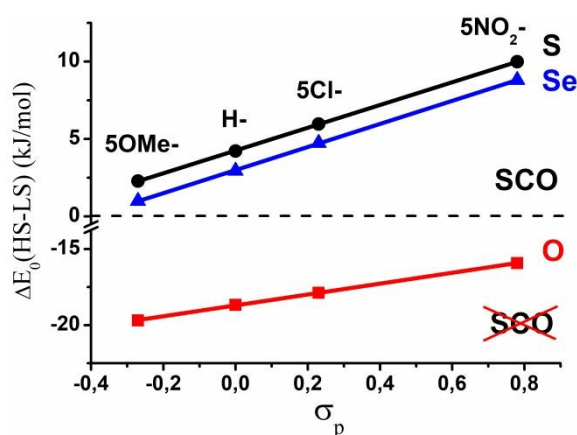


**Figure 7.** Dependence of the calculated (B3LYP\*/6-311 ++G (d,p)) difference of total energies between HS and LS states for the neutral complexes: (S, ●), (Se, ▲) and (O, ■) with different substituents (R) on Hammett parameter ( $\sigma_p$ ). The dashed line marks the boundary of the SCO possible area:  $\Delta E_0(HS-LS) > 0$  (SCO possible),  $\Delta E_0(HS-LS) < 0$  (SCO impossible, stable HS state).

The MO energies are lowering due to elongation of the Fe-N(A, B) and Fe-X(A, B) bonds induced by the geometry changes from the doublet (LS) spin state to the sextet (HS) spin state, since the  $e_g$ -like orbitals form antibonding overlaps with the N(A, B) and X(A, B) lone pair orbitals. As a result of these geometry changes, the sextet spin state becomes more energetically stable.<sup>42</sup>

Since a thermally induced SCO is an entropy driven process, the major contribution comes from changes in the intramolecular vibrations ( $S_{\text{vib}}$ ) and spin multiplicity LS $\rightarrow$ HS ( $S_{\text{el}} \sim 25\%$ ).<sup>2</sup> Therefore, the main criterion for the appearance of SCO is the energy proximity of the LS to HS state. The results of DFT calculations of total energy difference between HS and LS states ( $\Delta E_0(HS-LS)$ ) for the iron(III) neutral complexes of R-salicylaldehyde thio-, seleno-, semicarbazone are shown on the Figure 7 and Table S4. According to DFT calculations, the neutral complexes with  $S_2N_2O_2$  and  $Se_2N_2O_2$  coordination may experience the thermally induced spin transition, while  $N_2O_4$  coordination environment implies the stabilization of HS state of iron ion. All dependences demonstrate similar positive linear relationship between  $\Delta E_0(HS-LS)$  and "R" substituent Hammett parameter ( $\sigma_p$ ).<sup>43</sup> This also implies that iron/phenoxide  $\pi$ -bonding is important for these compounds. Electron-withdrawing substituents (5Cl-, 5NO<sub>2</sub>-) would strengthen the ligand field by reducing ligand-metal  $\pi$ -donation and stabilize the low-spin states of the complexes. Electron-donating substituents (5MeO-) on the contrary would weaken the ligand field by enhancing ligand-metal  $\pi$ -donation and stabilize the high-spin states of the complexes.<sup>44</sup> Thus, the regulation of spin transition parameter ( $T_{1/2}$ ) for these

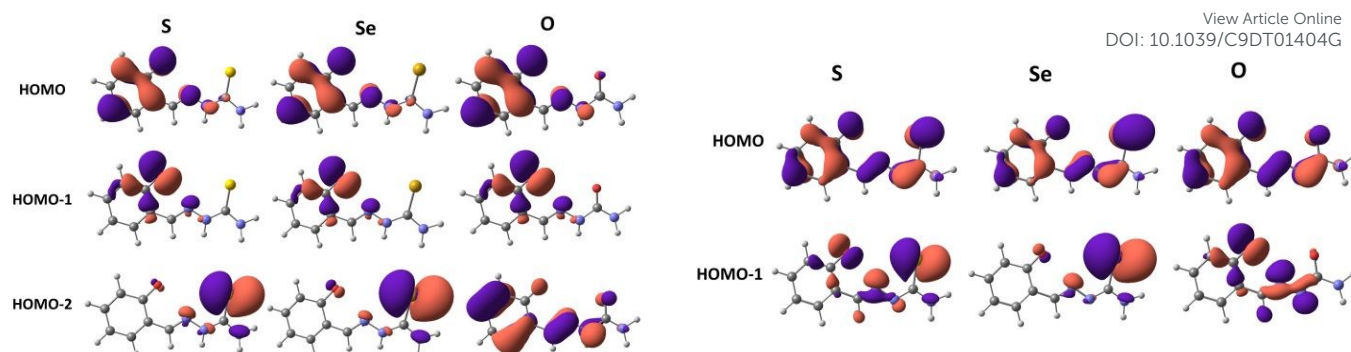


**Figure 8.** HOMO, HOMO-1 and HOMO-2 (left); HOMO, HOMO-1 (right) surfaces calculated (B3LYP\*/6-311++G(d,p)) for (A) (left) and (B) (right) ligand forms, based on the optimized structures coordinates of the Fe(III) neutral complexes (I) (X= O, S, Se; R=H) in the HS state. A contour of  $0.04 \text{ e}\text{\AA}^{-3}$  has been used for the MOs plots.

compounds can be realized by varying the substituents in benzene ring of salicylaldehyde. It's important to mention that the linear dependence (Figure 7) reflects only electronic influence of ligand substituents. Similar linear dependence was obtained for spin-crossover saltrien-type Fe(III) complexes, which contain analogous fragment of R-salicylaldehyde in their structure.<sup>44</sup> The observed correlation may vary under the influence of the crystal packing features.<sup>20</sup>

Magnetic measurement, carried out for  $[\text{Fe}(\text{Hsemsal})(\text{semsal})] \cdot 3\text{H}_2\text{O}$  complex, confirms results of DFT calculations. Noteworthy, the value of  $\Delta E_0$  (HS-LS) for the neutral complexes where X=S slightly exceeds for the neutral complexes where X=Se. The larger value of  $\Delta E_0$  (HS-LS) indicates the shift of  $T_{1/2}$  value towards higher temperatures. The similar experimental observation for Fe(III) anionic complexes was reported in previous works.<sup>11</sup>

The energy-level diagrams of the occupied  $\alpha$ -spin molecular orbitals for the HS Fe(III) neutral complexes (X=S, Se, O; R=H) are shown on the Figure S7. The observed distribution of the iron  $e_g$ -like and  $t_{2g}$ -like orbitals in MOs corresponds to calculated  $\Delta E_0$  (HS-LS) values (Table S4). However, the mixed iron d orbitals complicate detailed MO analysis for the complexes. The mixing of the iron d orbitals leads to the increase of the degree of the overlap between metal orbitals and  $\sigma$ -/ $\pi$ - donor ligand orbitals.<sup>45</sup>

The considered ligands include  $\pi$ -donor atoms: X= O, S and Se. Oxygen has higher electronegativity than sulfur and selenium. Therefore it has low-lying energy  $t_{2g}$ -orbitals what reduces iron d orbitals splitting energy. This fact correlates with the energy-level diagrams of MOs: iron  $t_{2g}^*$ -like orbitals of neutral complex with X=O are more destabilized compared to X=S and Se (Figure S7). The analysis of natural atomic charges on Fe for these complexes indicates that the degree of  $\pi$ -bonding in the complex with X=Se is stronger than in complex with X=S.<sup>46</sup> This corresponds to the smaller natural atomic charge on Fe(HS):  $0.781 e$  (X=S) >  $0.726 e$  (X=Se). A higher degree of  $\pi$ -bonding may also be the reason of value  $E_0$  (HS-LS) decreasing for the complex with X=Se. The observed energy discrepancy of the distribution of MOs containing iron  $t_{2g}^*$ -like orbitals for S and Se is the result of strong mixing of d orbitals.

The single-point calculations for the A and B ligand forms were also performed using the atomic coordinates clipped

from each optimized the Fe(III) neutral complexes in HS state. The N  $\sigma$ -like orbitals of ligand were observed in HOMO-1, HOMO-2 for A form and HOMO-1 for B form (Figure 8).

Here we conclude that  $\sigma$ -bonding of nitrogen atoms of imino ( $-\text{N}(\text{im})=$ ) groups have a little influence on the increase of iron d orbitals splitting energy, what provides the stabilization of HS state for neutral complexes with X=O (weak field ligand). The same example of the stabilization of HS state is observed for  $[\text{Fe}(\text{phsal})_2]^-$  anionic complex ( $\text{H}_2\text{phsal} = \text{N}$ -(2-hydroxyphenyl)salicylaldehyde) with  $\text{N}(\text{im})_2\text{O}_4$  coordinated environment. However  $[\text{Fe}(\text{azp})_2]^-$  and  $[\text{Fe}(\text{aznp})_2]^-$  complexes ( $\text{N}(\text{azo})_2\text{O}_4$  coordination) with azo ( $-\text{N}=\text{N}-$ ) group demonstrate SCO transition since  $\sigma$ -bonding of this groups with iron d orbitals leads to the enhancement of the ligand-field splitting energy (Figure S6).<sup>16</sup> The HOMO-1  $\sigma$ -type coefficients around the imino group in the B ligand form were much larger than in the A ligand form. Besides, these coefficients for the B ligand with X=S were slightly larger than in the case of X=Se while these coefficients for X=S and X=O are quite equal (Figure 8). Therefore, larger  $\sigma$ -type coefficients might result into the enhancement of the ligand-field splitting energy. This conclusion correlates with the calculated values of  $\Delta E_0$  (HS-LS) (Table S4). Moreover, iron  $e_g^*$ -like orbitals for the complex with X=S are more destabilized comparing to X=Se, since  $\text{thsa}^{2-}$  ligand has larger  $\sigma$ -type coefficients around the imino group (Figure S7).

To corroborate the results described above we performed analogous DFT calculations for the anionic forms of complexes (X= O, S, Se) with R=H, where Fe(III) is coordinated by two B ligands. Computation details are produced in the supporting information (Table S5). The  $\Delta E_0$  (HS-LS) values for anionic complexes increase in row: O(-11.05 kJ/mol)  $\rightarrow$  Se(9.80 kJ/mol)  $\rightarrow$  S(12.46 kJ/mol). Compared to the neutral complexes, the  $\Delta E_0$  (HS-LS) values for anionic complexes increase by 8.24 kJ/mol for X=S, 7.62 kJ/mol for X=O, and 6.86 kJ/mol for X=Se (Table S4). Thereby, the B form ligand gives much larger value of the ligand-field splitting energy because of the nitrogen atom of imino group has larger  $\sigma$ -type coefficients. Comparing to X=Se, B form ligand with X=S may also give larger values of  $\Delta E_0$  (HS-LS) due to larger  $\sigma$ -type coefficients of imino group (Figure 7). However, the higher value of  $\Delta E_0$  (HS-LS) = -11.05

kJ/mol for anionic complex with X=O does not provide the possibility of SCO transition.

## Conclusions

Neutral iron(III) complex [Fe(Hsemsal)(semsal)] · 3H<sub>2</sub>O (**1**) with N<sub>2</sub>O<sub>4</sub> coordination environment was synthesized. Crystal structure analysis showed that the Fe(III) ion in **1** has a distorted octahedral coordination of two nitrogen and four oxygen atoms owned by two tautomeric forms of the salicylaldehyde semicarbazone ligand: Hsemsal<sup>-</sup> (keto) and semsal<sup>2-</sup> (enol).

The magnetization measurements confirmed the persistence of the high spin state  $S = 5/2$  of Fe(III) ions in **1** down to liquid helium temperatures. Negative value of the Weiss temperature indicates the presence of weak antiferromagnetic interaction between magnetic centers in **1**.

The DFT calculations were performed for the iron(III) neutral complexes with salicylaldehyde thio-, seleno- and semicarbazone ligands. It was concluded that thermally induced spin transition may occur in the complexes with S<sub>2</sub>N<sub>2</sub>O<sub>2</sub> and Se<sub>2</sub>N<sub>2</sub>O<sub>2</sub> coordination environments while in the case of N<sub>2</sub>O<sub>4</sub> coordination the high spin state of iron ion is stabilized. The comparison of neutral and anionic forms (Scheme 1) of iron(III) complexes demonstrates that **B** form of ligand gives much larger value of the ligand-field splitting energy than **A** form. The replacement of sulfur atom by selenium atom does not lead to significant changes in the SCO properties of the complexes. The spin transition is displaced in a higher temperature range for S<sub>2</sub>N<sub>2</sub>O<sub>2</sub>-coordinated complexes in comparison with Se<sub>2</sub>N<sub>2</sub>O<sub>2</sub>-coordinated ones. The positive linear relationship between  $\Delta E_0$  (HS-LS) and Hammett parameter ( $\sigma_p$ ) indicates the iron/phenoxide  $\pi$ -bonding. Thus, the regulation of SCO parameter ( $T_{1/2}$ ) for these compounds can be realized by varying substituents in the benzene ring of salicylaldehyde.

The present study provides insight into the influence of X<sub>2</sub>N<sub>2</sub>O<sub>2</sub> coordination environment in the row X=O, S, Se on the SCO behavior of neutral and anionic iron(III) complexes. In addition, this material might be useful for developing synthetic strategies for the preparation of new spin-crossover systems based on tridentate ligands of salicylaldehyde carbazone family.

## Conflicts of interest

There are no conflicts to declare.

## Acknowledgements

The work was done on the topic of the State task (No. 0089-2019-0011) with using of the Analytical Center for Collective Use tool base and Computational Center of the IPCP RAS. Partially the study was carried out within the state assignment for the ISSP RAS. This work was supported partly by the Ministry of Education and Science of the Russian Federation in

the framework of Increase Competitiveness Program of NUST "MISIS" Grant No. K2-2017-084; by Act 211 of the Government of Russian Federation, Contracts No. 02.A03.21.0004 and No. 02.A03.21.0011, and Russian Foundation for Basic Research Grant No.18-32-00153.

## Notes and references

- 1 K. Takahashi, *Inorganics*, 2018, **6**, 32.
- 2 P. Gutlich and H. A. Goodwin, *Topics in Current Chemistry*, 2004, **233**, 1.
- 3 *Spin-Crossover Materials: Properties and Applications*, ed. M. A. Halcrow, A John Wiley & Sons, Ltd, Chichester, 2013, pp. 1–541.
- 4 O. Kahn, J. Kröber and C. Jay, *Adv. Mater.*, 1992, **4**, 718.
- 5 K. S. Kumar, M. Ruben, *Coord. Chem. Rev.*, 2017, **346**, 176.
- 6 J. Linares, E. Codjovi and Y. Garcia, *Sensors*, 2012, **12**, 4479.
- 7 D. J. Harding, P. Harding and W. Phonsri, *Coord. Chem. Rev.*, 2016, **313**, 38.
- 8 W. Phonsri, P. Harding, K. S. Murray, B. Moubaraki and D. J. Harding, *New J. Chem.*, 2017, **41**, 13747.
- 9 S. Floquet, M. C. Muñoz, R. Guillot, E. Rivière, G. Blain, J.-A. Réal and M.-L. Boillot, *Inorg. Chim. Acta.*, 2009, **362**, 56.
- 10 R. J. Laverick, A. B. Carter, H. A. Klein, A. J. Fitzpatrick, T. D. Keene and G. G. Morgan, J. A. Kitchen, *Inorg. Chim. Acta.*, 2017, **463**, 126.
- 11 V. V. Zelentsov, A. V. Ablov, K. I. Turta, R. A. Stukan, N. V. Gerbeleu, E. V. Ivanov, A. P. Bogdanov, N. A. Barba and V. G. Bodyu, *Rus. J. Inorg. Chem.*, 1972, **18**, 1929.
- 12 S. Kang, Y. Shiota, A. Kariyazaki, S. Kanegawa, K. Yoshizawa and O. Sato, *Chem. Eur. J.*, 2016, **22**, 532.
- 13 a) S. Floquet, M.-L. Boillot, E. Rivière, F. Varret, K. Boukheddaden, D. Morineau and P. Négrier, *New J. Chem.*, 2003, **27**, 341; b) S. Floquet, N. Guillou, P. Négrier, E. Rivière and M.-L. Boillot, *New J. Chem.*, 2006, **30**, 1621.
- 14 S. Floquet, E. Rivière, K. Boukheddaden, D. Morineau and M.-L. Boillot, *Polyhedron*, 2014, **80**, 60.
- 15 W. Phonsri, L. C. Darveniza, S. R. Batten and K. S. Murray, *Inorganics*, 2017, **5**, 51.
- 16 K. Takahashi, K. Kawamukai, M. Okai, T. Mochida, T. Sakurai, H. Ohta, T. Yamamoto, Y. Einaga, Y. Shiota and K. Yoshizawa, *Chem. Eur. J.*, 2016, **22**, 1253.
- 17 S. Murata, K. Takahashi, T. Sakurai, H. Ohta, T. Yamamoto, Y. Einaga, Y. Shiota and K. Yoshizawa, *Crystals*, 2016, **6**, 49.
- 18 D. Palanimuthu, Z. Wu, P. J. Jansson, N. Braid, P. V. Bernhardt, Des R. Richardson and D. S. Kalinowski, *Dalton Trans.* 2018, **47**, 7190.
- 19 N. M. Samus and V. G. Chebanu, *Rus. J. Inorg. Chem.*, 1969, **14**, 2089.
- 20 E. W. T. Yemeli, G. R. Blake, A. P. Douvalis, T. Bakas, G. O. R. A. van Ekenstein and P. J. van Koningsbruggen, *Chem. Eur. J.*, 2010, DOI: 10.1002/chem.201002100.
- 21 Z.-Y. Li, J.-W. Dai, Y. Shiota, K. Yoshizawa, S. Kanegawa and O. Sato, *Chem. Eur. J.*, 2013, **19**, 12948.
- 22 W. Phonsri, D. S. Macedo, C. G. Davies, G. N. L. Jameson, B. Moubaraki and K. S. Murray, *Dalton Trans.*, 2017, **46**, 7020.
- 23 Z.-Y. Li, J.-W. Dai, K. J. Gagnon, H.-L. Cai, T. Yamamoto, Y. Einaga, H.-H. Zhao, S. Kanegawa, O. Sato, K. R. Dunbar and R.-G. Xiong, *Dalton Trans.*, 2013, **42**, 14685.
- 24 a) Y.-M. Hao, *Acta Crystallogr. Sect. E.*, 2010, **66**, o2211. b) V. M. Leovac, L. Bjelica and L. Jovanovic, *Polyhedron*, 1985, **4**, 233.
- 25 T. G. Battye, L. Kontogiannis, O. Johnson, H. R. Powell and A. G. Leslie, *Acta Crystallogr. Sect. D*, 2011, **67**, 271.
- 26 P. R. Evans, *Acta Crystallogr. Sect. D*, 2006, **62**, 72.

- 27 G. M. Sheldrick, *Acta Crystallogr. Sect. C*, 2015, **71**, 3.
- 28 O. V. Dolomanov, L. J. Bourhis, R. J. Gildea, J. A. K. Howard and H. Puschmann, *J. Appl. Crystallogr.*, 2009, **42**, 339.
- 29 D. M. Kheiker, M. V. Kovalchuk, V. N. Korchuganov, Y. N. Shilin, V. A. Shishkov, S. N. Sulyanov, P. V. Dorovatovskii, S. V. Rubinsky and A. A. Rusakov, *Crystallogr. Reports*, 2007, **52**, 1108.
- 30 A. P. Hammersley, *ESRF Internal Report*. FIT2D V9.129 Reference Manual V3.1. 1998.
- 31 V. Petříček, M. Dušek and L. Palatinus, *Zeitschrift Für Kristallographie - Cryst. Mat.*, 2014, **229**, 345.
- 32 M. J. Frisch, G. W. Trucks, H. B. Schlegel, G. E. Scuseria, M. A. Robb, J. R. Cheeseman, G. Scalmani, V. Barone, B. Mennucci, G. A. Petersson, H. Nakatsuji, M. Caricato, X. Li, H. P. Hratchian, A. F. Izmaylov, J. Bloino, G. Zheng, J. L. Sonnenberg, M. Hada, M. Ehara, K. Toyota, R. Fukuda, J. Hasegawa, M. Ishida, T. Nakajima, Y. Honda, O. Kitao, H. Nakai, T. Vreven, J. A. Montgomery, Jr., J. E. Peralta, F. Ogliaro, M. Bearpark, J. J. Heyd, E. Brothers, K. N. Kudin, V. N. Staroverov, T. Keith, R. Kobayashi, J. Normand, K. Raghavachari, A. Rendell, J. C. Burant, S. S. Iyengar, J. Tomasi, M. Cossi, N. Rega, J. M. Millam, M. Klene, J. E. Knox, J. B. Cross, V. Bakken, C. Adamo, J. Jaramillo, R. Gomperts, R. E. Stratmann, O. Yazyev, A. J. Austin, R. Cammi, C. Pomelli, J. W. Ochterski, R. L. Martin, K. Morokuma, V. G. Zakrzewski, G. A. Voth, P. Salvador, J. J. Dannenberg, S. Dapprich, A. D. Daniels, O. Farkas, J. B. Foresman, J. V. Ortiz, J. Cioslowski, and D. J. Fox, *Gaussian 09, Revision B. 01*, Gaussian, Inc., Wallingford CT, 2010.
- 33 M. Reiher, *Inorg. Chem.*, 2002, **41**, 6928.
- 34 A. D. Becke, *J. Chem. Phys.*, 1993, **98**, 5648.
- 35 C. Lee, W. Yang and R. G. Parr, *Phys. Rev. B: Condens. Matter Mater. Phys.*, 1988, **37**, 785.
- 36 H. Paulsen and A. X. Trautwein, *Topics in Current Chemistry*, 2004, **235**, 197.
- 37 J. A. Pople, M. Head-Gordon and K. Raghavachari, *J. Chem. Phys.*, 1987, **87**, 5968.
- 38 E. D. Glendening, J. K. Badenhoop, A. E. Reed, J. E. Carpenter, J. A. Bohmann, C. M. Morales, and F. Weinhold, NBO 3.1, Theoretical Chemistry Institute, University of Wisconsin, Madison, WI, USA, 2001.
- 39 L. J. Bellamy, *The Infrared Spectra of Complex Molecules*. Methuen, London, 1959, p. 108.
- 40 G. A. Bain and J. F. Berry, *J. Chem. Education.*, 2008, **85**, 532.
- 41 R. L. Carlin and A. J. van Duyneveldt, *Magnetic properties of transition metal compounds*, Springer-Verlag Berlin Heidelberg, 1977, p. 28.
- 42 H. Ando, Y. Nakao, H. Sato and S. Sakaki, *J. Phys. Chem. A*, 2007, **111**, 5515.
- 43 C. Hansch, A. Leo and R. W. Taft, *Chem. Rev.*, 1991, **91**, 165.
- 44 M. A. Halcrow, *Crystals*, 2016, **6**, 58.
- 45 J. P. Holland and N. Vasdev, *Dalton Trans.*, 2014, **43**, 9872.
- 46 J. Conradie, *S. Afr. J. Chem.*, 2010, **63**, 65.

View Article Online  
DOI: 10.1039/C9DT01404G

Dalton Transactions Accepted Manuscript

## Table of Contents

View Article Online  
DOI: 10.1039/C9DT01404G



A novel neutral complex  $[Fe^{III}(Hsemsal)(semsal)] \cdot 3H_2O$  was synthesized and its magnetic properties, crystal and electronic structure were studied.